International Journal of
Geo-Information

Article

Investigating the Relationship between the Built Environment and Relative Risk of COVID-19 in Hong Kong

Jianwei Huang [1], Mei-Po Kwan [1,2,*], Zihan Kan [1], Man Sing Wong [3,4], Coco Yin Tung Kwok [3] and Xinyu Yu [3]

1 Institute of Space and Earth Information Science, The Chinese University of Hong Kong, Hong Kong, China; jianwei.huang@link.cuhk.edu.hk (J.H.); zihankan@cuhk.edu.hk (Z.K.)
2 Department of Geography and Resource Management, The Chinese University of Hong Kong, Hong Kong, China
3 Department of Land Surveying and Geo-Informatics, The Hong Kong Polytechnic University, Hung Hom, Hong Kong, China; lswong@polyu.edu.hk (M.S.W.); yt-coco.kwok@connect.polyu.hk (C.Y.T.K.); xin-yu.yu@connect.polyu.hk (X.Y.)
4 Research Institute for Sustainable Urban Development, The Hong Kong Polytechnic University, Hung Hom, Hong Kong, China
* Correspondence: mpkwan@cuhk.edu.hk

Received: 20 September 2020; Accepted: 22 October 2020; Published: 25 October 2020

Abstract: Understanding the relationship between the built environment and the risk of COVID-19 transmission is essential to respond to the pandemic. This study explores the relationship between the built environment and COVID-19 risk using the confirmed cases data collected in Hong Kong. Using the information on the residential buildings and places visited for each case from the dataset, we assess the risk of COVID-19 and explore their geographic patterns at the level of Tertiary Planning Unit (TPU) based on incidence rate (R1) and venue density (R2). We then investigate the associations between several built-environment variables (e.g., nodal accessibility and green space density) and COVID-19 risk using global Poisson regression (GPR) and geographically weighted Poisson regression (GWPR) models. The results indicate that COVID-19 risk tends to be concentrated in particular areas of Hong Kong. Using the incidence rate as an indicator to assess COVID-19 risk may underestimate the risk of COVID-19 transmission in some suburban areas. The GPR and GWPR models suggest a close and spatially heterogeneous relationship between the selected built-environment variables and the risk of COVID-19 transmission. The study provides useful insights that support policymakers in responding to the COVID-19 pandemic and future epidemics.

Keywords: risk of COVID-19; built environment; global Poisson regression; geographically weighted Poisson regression

1. Introduction

Three coronaviruses have emerged in the past two decades (i.e., SARS-CoV, MERS-CoV, and SARS-CoV-2) [1]. Among them, the novel coronavirus (SARS-CoV-2) and the COVID-19 pandemic it causes pose a particularly serious threat to global health, as the numbers of new COVID-19 cases and deaths continue to increase at alarming rates in some countries. COVID-19 was designated as a pandemic by the World Health Organization (WHO) on 11 March 2020 [2]. To mitigate the pandemic and control its spread in human populations, most governments have implemented drastic intervention measures, which include travel restrictions, stay-at-home orders, school closings, and restrictions of public gatherings [3–5]. These control strategies seek to mitigate the spread of COVID-19 by forcing or encouraging people to practice social distancing and reducing risky social interactions.

Measures like social distancing, travel restrictions, and stay-at-home orders are non-pharmaceutical interventions for controlling the spread of COVID-19 by reducing the close contact among people and changing their behaviors [6]. Several studies have observed the benefits of non-pharmaceutical interventions for controlling pandemics. These studies found that changes in individual behavior can have large effects on reducing the transmission of infectious disease [7–11]. The benefits of human behavioral changes via social distancing seem obvious. However, human behavior may change in ways that lead to opposite consequences during a pandemic since human behavior is also shaped by the built environment [12,13]. For instance, people still need to obtain groceries, medicines, and essential services during a pandemic. Further, some people may still want to conduct certain outdoor activities (e.g., hiking, picnicking, or taking beach vacations) or social activities at different venues or places to maintain their mental health during long stay-at-home orders [14,15]. Hence, it is critical to investigate the relationship between the built environment and COVID-19 transmission risk in order to effectively control the pandemic. On one hand, the new knowledge generated can inform the development and enhance the effectiveness of non-pharmaceutical interventions by identifying more targeted strategies to reduce people's risky contact with others. Further, informing people to avoid conducting high-risk activities and visiting high-risk places would help generate the behavioral changes for mitigating the spread of infectious diseases. On the other hand, certain features of the built environment can be modified or dynamically managed to promote healthy behaviors and reduce the risk of contracting COVID-19 during the pandemic.

This study thus investigates the relationship between built-environment features and COVID-19 transmission risk in Hong Kong. It seeks to answer the following questions: (1) What are the key geographic patterns of the COVID-19 cases in Hong Kong? (2) What built-environment features and areas are associated with a higher risk of COVID-19 transmission in the study area? To answer these questions, we first assess COVID-19 risk using two different indicators derived from the data on COVID-19 cases and their locations available on the Hong Kong Department of Health COVID-19 webpage. The first indicator is incidence rate (R1: case density) which is calculated based on the number of confirmed cases per 1,000 people in each of the Tertiary Planning Units (TPU) in Hong Kong. The second one is venue density (R2), which is computed based on the number of venues or buildings visited by the confirmed cases in each TPU. Then, the spatial distribution and the frequency distributions of R1 and R2 are analyzed. Finally, we use global Poisson regression (GPR) and geographically weighted Poisson regression (GWPR) to investigate the relationship between certain built-environment features and COVID-19 risk. The results show that COVID-19 risk declines dramatically over space from the TPUs with the highest risk, indicating that the risk of COVID-19 transmission tends to be concentrated in particular areas of Hong Kong. Furthermore, the rate of decay for R1, as reflected by the frequency distribution of the incidence rate, is greater than that of R2. This implies that the incidence rate indicator may underestimate the risk of COVID-19 in some suburban areas. The adjusted percent deviance explained of the GPR model is 0.44 for R1 and 0.58 for R2, which suggests a close relationship between the built-environment variables and COVID-19 risk. The GWPR models perform better than the GPR regression models, and the results indicate that the relationships between the selected built-environment variables and COVID-19 risk (i.e., R1 and R2) vary spatially across the study area.

2. The Built Environment and the Spread of Infectious Disease

At the time of writing, COVID-19 has become a global pandemic that constitutes a serious threat to public health in many countries, and Hong Kong is experiencing a rampant third wave of the pandemic. Past studies have found that local built-environment features and people's socioeconomic characteristics significantly influence viral transmission and incidence rates [16]. On one hand, the built environment heavily influences the space–time patterns and intensity of people's social interactions.

The location, density, and accessibility of different built-environment features (e.g., subway stations) may affect the density of people moving through certain spaces and thus may have a significant impact on disease transmission (e.g., higher built-environment densities tend to increase people's interactions) [17]. Different types of housing and the amount of green space in an area (which facilitates social distancing and the avoidance of crowdedness) may also be important factors. Specific types of venues and areas where superspreading events and cluster outbreaks tend to occur (e.g., pubs, restaurants, and karaoke venues) are also high-risk built-environment features for disease transmission.

Our knowledge about the influences of the built and social environments on the spread of highly contagious infectious diseases like COVID-19 is still highly limited to date, and some apparently useful findings from recent studies may be unreliable. For instance, in a recent study of 913 metropolitan counties in the U.S., Hamidi et al. [18] found that metropolitan size is more important than density in influencing the spread of the COVID-19 pandemic in the U.S., based on county-based COVID-19 infection and mortality rates. But this finding is contrary to the results we obtained using much smaller areal units on the COVID-19 pandemic in Hong Kong; urban density seems to be an important factor affecting the incidence rate and transmission risk of COVID-19. An important methodological issue ignored in Hamidi et al. [18] is that whether density matters may depend on the spatial scale of the analytical units or geographic areas (e.g., counties, census tracts, or census block groups) used in the analysis. This is the well-known modifiable areal unit problem (MAUP), which means that research findings may vary due to the use of different spatial scales or zonal schemes of the geographic areas for deriving the area-based variables (e.g., urban density and infection rates).

Further, studies have found that the coronavirus can survive on various specific environmental surfaces for a long time outside of its host organism [19]. For instance, Casanova et al. [20] observed that the coronavirus can remain infectious in water and sewage for days to weeks. In 2003, a clustered outbreak of SARS-CoV happened in a high-rise residential building in Hong Kong through the faulty and contaminated sewage system of the building [21]. Van et al. [22] reported that the SARS-CoV-2 virus can remain in aerosols after 3 hours and on plastic and stainless-steel surfaces after 72 hours. The various built-environment surfaces on which the coronavirus can survive are distributed among various venues (e.g., pubs and restaurants) across urban spaces, and infected individuals may leave the virus on certain surfaces (e.g., door handles, elevator buttons, and tableware) in the venues they visited or stayed (e.g., restaurants or hotels). Hence, many built-environment features that allow people to carry out their daily activities may become potential sources of infection transmission [23,24].

Many studies have investigated the relationship between the built environment, human behavior, and health [25–28]. For instance, researchers have observed that neighborhoods with healthy and diverse food environments can reduce the incidence of obesity [29,30]. Dense green spaces, lower building height, and a good sky view may encourage people to undertake more outdoor activities (e.g., running, walking, cycling, picnicking, and hiking) and may lead to better health [31,32]. People's immunity may improve as a result of more physical activities and exposures to green spaces, which in turn may reduce stress, obesity, and vulnerability to infectious disease [33,34]. These findings are relevant to studies on COVID-19 risk because people with poor health are more vulnerable and more easily infected, which often manifest in certain patterns of comorbidities (e.g., people with chronic diseases like diabetes and hypertension are far more likely to die from COVID-19). On the other hand, studies have found that people tend to visit areas with high accessibility and high-density commercial areas for social activities with their friends (e.g., drinking in bars, watching movies, and dining in restaurants) to reduce their stress [35,36]. Further, areas with high-density transport facilities and diverse land-use types may encourage people to conduct more short-distance travel activities due to the convenience of activity opportunities [37].

On the whole, these studies highlight that the spatial distribution of built-environment features influences the geographic patterns of not only human contacts and social interactions but also people's health and immunity (by increasing certain health-promoting activities, which in turn may modify people's COVID-19 risk). This suggests that the risk of contracting COVID-19 may be reduced by modifying risky human behaviors through modifying their interaction patterns (e.g., stay-at-home orders) and certain features of the built environment [38]. For instance, the nodal accessibility of an area, which represents how well the area is connected with other areas via the transport network, can be dynamically modified (e.g., travel restrictions) to help control the spread of a pandemic [39,40]. In the long run, improving urban designs and restructuring urban spaces (e.g., including more green spaces in high-density areas) may modify pedestrian flows and the concentrations of activities in certain areas, which may help mitigate the spread of future pandemics [41]. Hence, the geographic patterns of human behaviors and interactions can be modified using built-environment-related non-pharmaceutical intervention measures to control the spread of COVID-19 [42]. It is thus important to first understand the transmission dynamics of COVID-19 by examining the relationships among built-environment features and COVID-19 risk.

3. Data and Methods

3.1. Study Area and Data

As the study area of this research, Hong Kong is a special administrative region of China in the eastern Pearl River Delta (Figure 1). It is one of the most densely populated cities in the world. It has an estimated population of about 7.4 million (by the end of 2019) of various nationalities in a 1104 km^2 territory. This study seeks to shed light on the relationships between COVID-19 risk and built-environment features that may differ from other previous studies or other study areas [43,44]. It examines the spatially heterogeneous influences of various built-environment features on COVID-19 transmission risk in Hong Kong.

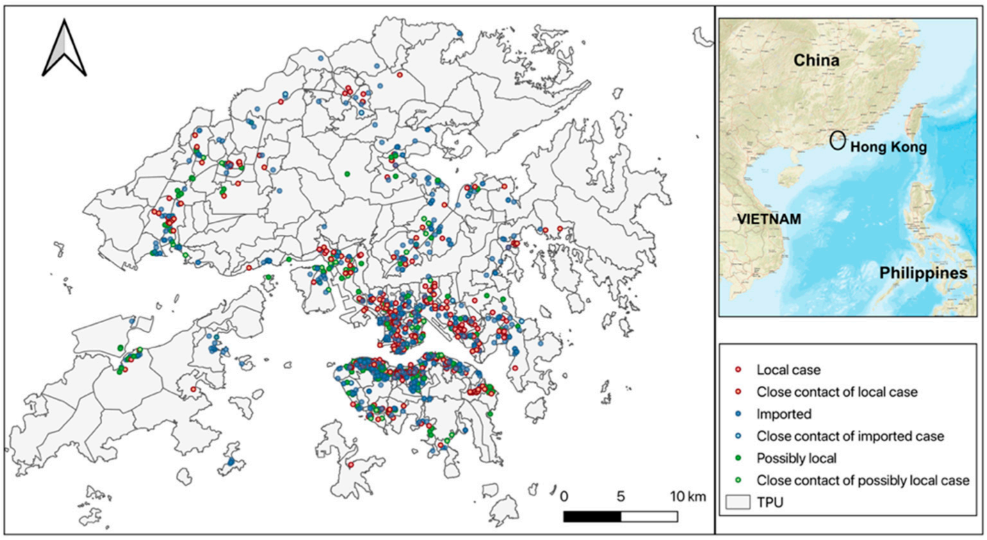

Figure 1. Study area and the residential spatial distribution of the confirmed cases (TPU, Hong Kong Tertiary Planning Unit).

The study uses the COVID-19 data provided by the Hong Kong Department of Health that are freely available via the government's open-data website (https://data.gov.hk). These data provide the following information about the COVID-19 cases in Hong Kong: the number of confirmed cases, a brief history and some demographic data for each case, and the countries, buildings, or venues visited by the cases during the incubation period for both imported and local cases. The confirmed cases are classified into two groups according to the geographic origin of infection: (1) imported cases (individuals who were infected in a foreign country or city) and (2) local cases, which include cases with clearly local sources (e.g., infected by a family member or a colleague at work), and cases involving infection by local or imported cases or by possible close contact with local or imported cases (see Figure 1). The Hong Kong Government started releasing the COVID-19 data from 27 January 2020, and the data have been updated daily after that. Furthermore, the first wave (i.e., most of the cases are imported cases) and the second wave (i.e., most of the cases are local cases) of the pandemic in Hong Kong had been under control by 14 April 2020 (i.e., no more local cases were found for several weeks after 14 April 2020). Hence, our analysis uses the data between 27 January 2020, and 14 April 2020 (which demarcate a period with two clear and complete waves of the pandemic) and is based on the 291 Tertiary Planning Units (TPUs) of Hong Kong and the specific buildings or venues visited by the confirmed cases (note that Hong Kong is divided into 291 TPUs for the purpose of town planning and census).

Using the building location information in the COVID-19 data, we first aggregate the case locations into the TPUs. Data on the relevant built-environment features of Hong Kong are then assembled from the same government open-data website (https://data.gov.hk) provided by various government departments (e.g., the Planning Department and the Transport Department). These data cover land use, population, building footprints, the multimodal transportation network, green spaces, transport facility density, and other features. The land-use dataset was compiled by the Planning Department in 2018 using multiple data sources (e.g., satellite images, in-house survey data, and other relevant information from various government departments), which is a 10 × 10 m raster dataset with 27 land-use types. Figure 2 shows an example of the data that includes various types of land use. The 2020 estimated population distribution was released by the Working Group on Population Distribution Projections (WGPD), which adopted the latest Census and Statistics Department's population projections released in September 2017 as the control. The building polygons are available as a 3D spatial dataset with building geometry and height. The multimodal transportation network dataset (as of 9 March 2020) includes data on the public transit routes and the location of public transit stations and stops (i.e., buses, the Mass Transit Railway, and ferries). Further, a sky-view factor (SVF) distribution dataset generated in a previous study is obtained from the authors [45]. This SVF dataset is a 10 × 10 m raster dataset retrieved from airborne LiDAR data. The SVF is the ratio of the visible sky with obstructions to that without obstruction, which ranges from zero to one to indicate a totally obstructed sky and open sky [46]. It has been found that the SVF is influenced by building height and density, which may in turn influence the health risk of an urban area [47]. Figure 3 shows the building polygons with height information and the spatial distribution of the sky-view factor.

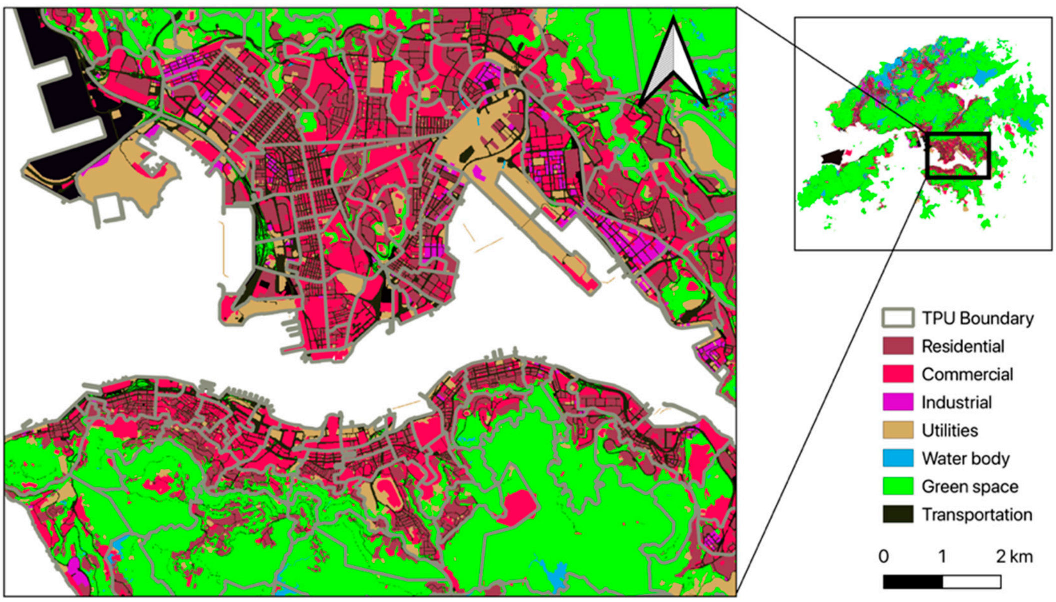

Figure 2. Land-use dataset.

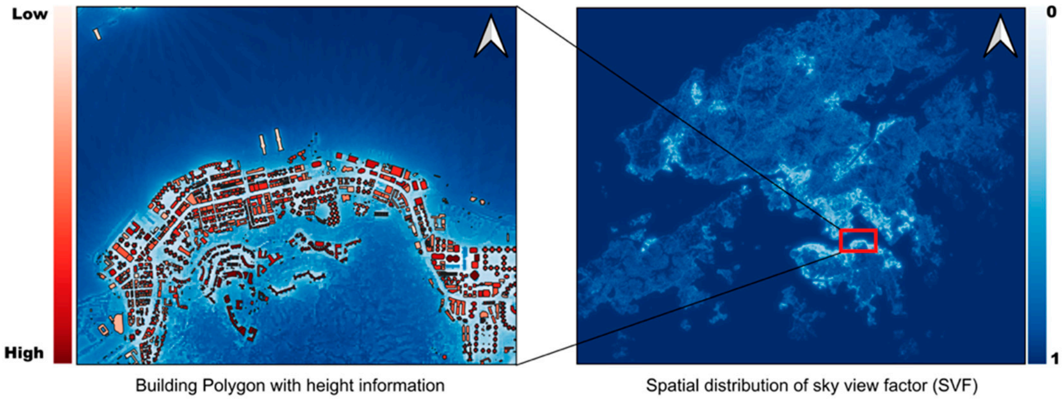

Figure 3. The building polygon and sky-view factor (SVF) datasets.

3.2. Assessing COVID-19 Risk

We use two different measures to assess the COVID-19 risk in Hong Kong. The first measure is the incidence rate or prevalence (R1: case density), which is the number of confirmed cases per 1000 people in each of the 291 Tertiary Planning Units (TPUs) over a specified time period. Note that only "local" confirmed cases are included to calculate the incidence rate in this study because imported cases are the result of the risk factors in their source areas, not the built-environment risk factors of Hong Kong. The second measure is R2 (venue density), which is the number of venues or buildings visited by the confirmed cases in each TPU. As mentioned earlier, the coronavirus can survive on various built-environment surfaces, and certain built-environment features tend to attract more human activities and interactions and thus are more likely to become sources of COVID-19 transmission. Hence, the second measure COVID-19 risk (R2) is computed based on the number of places and venues visited by all confirmed cases (i.e., buildings or places visited by confirmed cases in the last 14 days). Note that both "local" and "imported" confirmed cases are included when calculating R2 because the measure identifies the high-risk places or venues (which have been visited by confirmed cases and as a result, other people who visited these places have a higher risk of contracting COVID-19). The formula for R2 is as follows:

$$R2_s = \sum_{i \in T_s} w_i \quad (1)$$

where $R2_s$ is the venue density of TPU T_s, and w_i is the number of buildings or places in TPU T_s that have been visited by confirmed cases. TPUs with higher values of R1 and R2 have higher COVID-19 risk (i.e., their built-environment features and human activity patterns are more conducive to COVID-19 transmission).

3.3. Deriving the Built-Environment Features

As shown in Table 1, nine built-environment features are selected as the independent variables in our analysis: nodal accessibility (NA), population density (PD), private residential density (PR), commercial density (CD), green space density (GSD), building height (BH), transport facility density (TF), land-use diversity (LUD), and sky view (SV). They are computed for each of the 291 TUPs of Hong Kong based on the land-use data, population census data, building polygon data, multimodal transportation network data, and the SVF dataset described earlier. These nine built-environment features are described as follows.

The nodal accessibility of a TPU is derived based on the multimodal transport stations in each TPU. First, each public transit station (i.e., a metro, bus, or ferry station) is regarded as a node, where a link connects node n and m according to the route network. A specific recommendation from Alexander et al. [48] is that the distance between two stations for a transfer trip should not exceed 183 m (e.g., Lee et al. [49] connected bus stops for internode transfers within a distance of shorter than 120 m in Seoul). Hence, we add a transfer link that connects nearby nodes n and m of different transport modes if the distance between these two stations is not more than 100 m. Second, we create a connectivity matrix C, where C_{mn} presents all the links between nodes n and m (i.e., C_{mn} = 1 if node n and m are connected or 0 if node n and m are not connected). Note that there may be l shortest paths between nodes n and m. Assume that a path connects l_i stations via $k-1$ nodes with p modal transfers, then the connectivity between nodes n and m is estimated as follows:

$$C_{mn}^{(k)} = \sum\nolimits_{k=1}^{k_{max}} S^k \sum_{l_1,l_2,l_3\ldots l_{k-1}} C_{ml_1} C_{l_1 l_2} C_{l_2 l_3 \ldots} C_{l_{k-1} n} t^p \tag{2}$$

where t ($0 < t < 1$) is the scalar measure of the ineffectiveness of transfer, and S ($0 < S < 1$) represents the scalar of the distance-decay effect. In this study, t is 0.7 and S is 0.8 based on the results of a previous study [50]. After estimating the connectivity between each pair of nodes, the nodal accessibility of node m is obtained by summing the total connectivity C_{mn} over all n:

$$C_m = \sum_n C_{mn} \tag{3}$$

Finally, the nodal accessibility of a TPU is derived by summing up the nodal accessibility of all the public transit stations in that TPU.

Table 1. Explanations of the abbreviations for the built-environment variables.

Name	Abbreviations	Dependent Variables
Nodal accessibility	NA	R2
Population density	PD	R1 and R2
Private residential	PR	R1 and R2
Commercial density	CD	R2
Green space density	GSD	R2
Building height	BH	R1
Transport facility density	TF	R1
Land-use diversity	LUD	R1
Sky view	SV	R2

Population density (PD) is the number of people per kilometer in each TPU. Private residential density (PR), commercial density (CD), transport facility density (TF), and green space density (GSD) are computed based on the area of each of these land-use types in each TPU divided by the area of that TPU. Note that green space density (GSD) in each TPU is estimated based on the sum of the area of grassland, shrubland, and woodland, which cover about 65.4% of the total land-use area of Hong Kong. This area is calculated based on the land-use data mentioned earlier, which classify a cell's land use as green space (i.e., grass, woodland, and shrubland) if the cell is covered dominantly by vegetation. Land-use diversity (LUD) is estimated using the following widely used entropy model:

$$LUD = -\sum_{i=1}^{n} \frac{p_i * \ln p_i}{n} \tag{4}$$

where p_i represents the proportion of the ith land-use type, and n is the total number of land-use types. Building height (BH) is estimated using the building polygon data and digital topographic information. In this analysis, building height refers to the average building height for each TPU. Sky view (SV) refers to the average SVF per km^2 in each TPU, which is the total SVF in each TPU divided by the area of that TPU.

3.4. Exploring the Relationship between Built-Environment Features and COVID-19 Risk

Given that the risk of COVID-19 (i.e., R1 and R2) mentioned in Section 3.2 are count data and that the Poisson regression model is a suitable technique for modeling count data [51], we thus use both global Poisson regression (GPR) and geographically weighted Poisson regression (GWPR) to investigate the relationship between built-environment features and COVID-19 risk. In this analysis, R1 and R2 are the dependent variables, and the independent variables are the nine built-environment features. The GPR and GWPR models are estimated based on the TPUs as the units of analysis. The GPR model is formulated as follows:

$$ln(Ri) = \beta_0 + \beta_1 NA + \beta_2 PD + \beta_3 PR + \beta_4 CD + \beta_5 GSD + \beta_6 BH(or\ SV) + \varepsilon \tag{5}$$

where Ri represents the COVID-19 risk of TUP i, β_i denotes the regression coefficients for the intercept term and the independent variables, and ε denotes the random error. The GWPR model was developed to take into account the issues that the relationships between variables may vary over space, which is referred to as spatial nonstationarity [52], and to reduce estimation error due to spatial autocorrelation. The GWPR model is a localized model that captures the spatial variations in the relationships between variables by fitting parameters that vary over space, weighting relevant neighboring observations (which are TPUs in this study) by using a spatial weight matrix. In this study, the GWPR model is formulated as follows:

$$\begin{gathered} ln(Ri) = \beta_0(u_i) + \beta_1(u_i)NA + \beta_2(u_i)PD + \beta_3(u_i)PR + \beta_4(u_i)CD + \beta_5(u_i)GSD \\ +\beta_6(u_i)BH(or\ SV) + \varepsilon \end{gathered} \tag{6}$$

where i represents the ith TPU, R_i stands for the COVID-19 risk of the ith TPU, β_i is the estimated regression coefficients of the ith TPU, and ε_i is the error term for TPUi. Note that β_j is now a function of location $ui = (uxi, uyi)$, which denotes the two-dimensional coordinates of the ith point (the centroid of the ith TPU) in space. Thus, spatial nonstationarity is addressed in the GWPR modeling framework. In this modeling effort, spatially adaptive bandwidth values are obtained by using the method that minimizes the Akaike information criterion (AIC) of regression models. The variance inflation factor (VIF) is used to test the multicollinearity of the variables. The Akaike information criterion (AIC) approach is used to evaluate the tradeoff between the goodness of fit and the simplicity of the models (i.e., to assess the risk of overfitting or underfitting).

4. Results

4.1. Assessing the COVID-19 Risk in Each TPU

In this subsection, we explore the characteristics of COVID-19 risk in Hong Kong based on the two measures described in Section 3.2. Recall that the first measure is the incidence rate or prevalence (R1: case density), which is the number of confirmed cases per 1000 people in each of the 291 Tertiary Planning Units (TPUs) over a specified time period. The second measure is R2 (venue density), which is the number of venues or buildings visited by the confirmed cases in each TPU.

Figure 4 presents the frequency distribution of COVID-19 risk at the TPU level. Both the frequency distributions of R1 and R2 among the 291 TPUs in Hong Kong declines dramatically, indicating that COVID-19 risk is concentrated in the top few TPUs. In order to understand the decay effects in the frequency distributions of R1 and R2, we fit two probability distribution curves using the exponential function $p(x) \sim e^{bx}$ and the power-law function $p(x) \sim x^b$ to the distributions. The results indicate that both R1 and R2 have a better fit to the exponential function (i.e., $R^2 = 0.97$ for R1 and $R^2 = 0.98$ for R2) than to the power-law function (i.e., $R^2 = 0.88$ for R1 and $R^2 = 0.91$ for R2). Further, the rate of decay for R1 is higher than that for R2, reflecting that the number of TPUs with high R1 is smaller than R2.

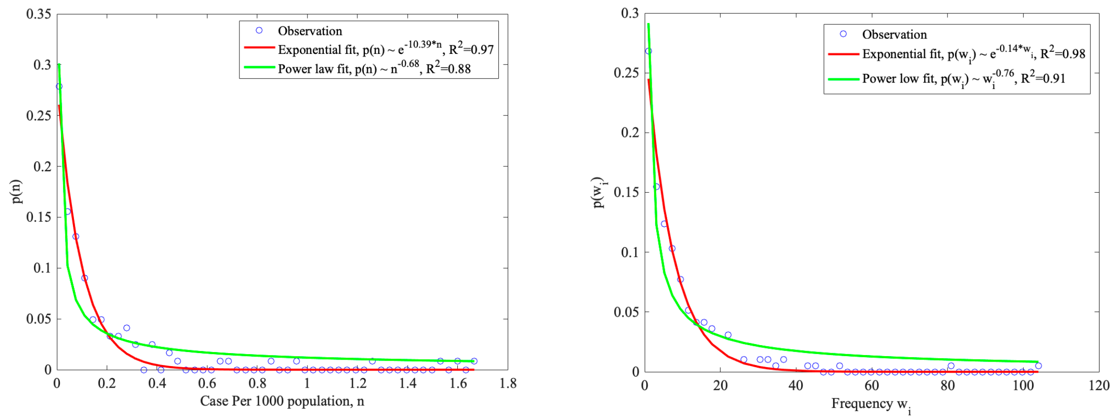

(**a**) (**b**)

Figure 4. The frequency distribution of COVID-19 risk in Hong Kong: (**a**) The frequency distribution of R1; (**b**) The frequency distribution of R2.

Figure 5 shows the spatial distribution of COVID-19 risk in Hong Kong at the TPU level. As indicated by the results of the frequency distribution analysis of R1 and R2, areas with a high COVID-19 risk are concentrated in a few TPUs in Hong Kong. With respect to the spatial distribution of R1 (Figure 5a), there are three areas (marked as A, B, and C) with high R1. Specifically, Area A is the downtown area with a high density of population and commercial buildings. Areas B and C are suburban areas with low population density and large amounts of public spaces (e.g., country parks and beaches). Figure 5b displays the spatial distribution of R2, where six areas (marked as A, B, C, D, E, and F) with high R2 are identified. Specifically, Areas A and B have high-density commercial and residential buildings, while Areas C, D, E, and F are suburban areas with large amounts of open space (e.g., country parks and beaches). These results suggest that both the downtown and certain suburban areas in the city are high COVID-19 risk areas. Moreover, the incidence rate indicator (R1) may underestimate the COVID-19 risk in some suburban areas with a considerable amount of public spaces.

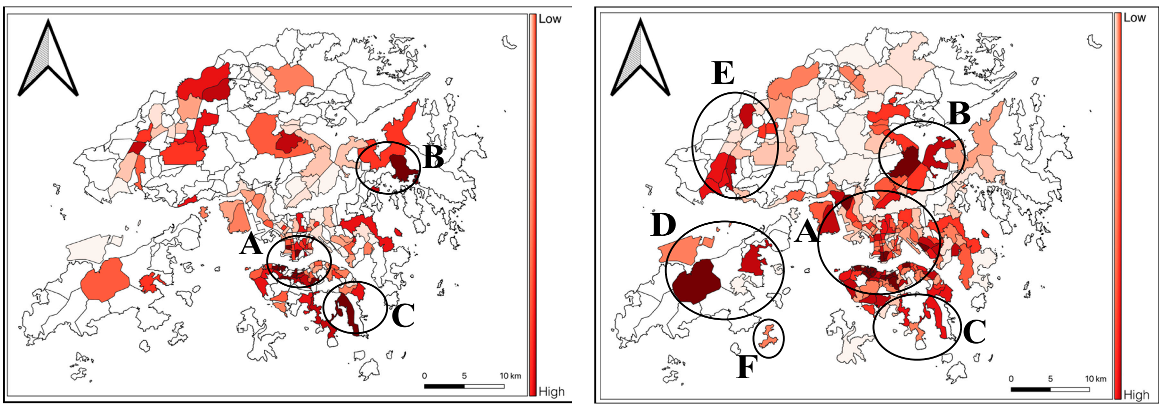

(**a**) (**b**)

Figure 5. Spatial distribution of COVID-19 risk in Hong Kong: (**a**) Spatial distribution of R1; (**b**) Spatial distribution of R2.

4.2. The Relationship between Built-Environment Features and COVID-19 Risk: Results of the GPR Analysis

In this subsection, we explore the relationships between selected built-environment variables and COVID-19 risk in the study area. The nine built-environment variables described in Section 3.3 are used as the independent variables in the following global Poisson regression (GPR) and geographically weighted Poisson regression (GWPR) analysis, and R1 and R2 are the dependent variables in separate models (see Table 2). Note that population density and building height are rescaled and standardized to a range from 0 to 1 in the GPR and GWPR models.

Table 2. Descriptive statistics of the independent variables and dependent variables.

	Abbreviations	**Mean**	**Standard Deviation**
Independent variables			
Nodal accessibility	NA	0.20	0.23
Population density	PD	30,042.00	40,741.63
Private residential	PR	0.08	0.11
Commercial density	CD	0.03	0.06
Green space density	GSD	0.42	0.34
Building height	BH	22.71	16.04
Transport facility density	TF	0.13	0.13
Land-use diversity	LUD	0.61	0.18
Sky view	SV	0.78	0.14
Dependent variables			
Risk 1	R1	0.18	0.23
Risk 2	R2	11.97	13.21

Two GPR models with R1 or R2 as the dependent variable are estimated to examine the global relationships between the built-environment variables and COVID-19 risk, respectively, in Hong Kong. The regression results are presented in Table 3. As the results indicate, the values of the variance inflation factor (VIF) of the independent variable are less than 10, indicating that there is no multicollinearity among the variables. Transport facility density, population density, private residential density, land-use diversity, and building height are significantly associated with R1. Meanwhile, nodal accessibility, population density, private residential density, commercial density, green space density, and sky view are significantly associated with R2. The ratios of residual deviance to degrees of freedom are 1.01 and 1.03 for R1 and R2, suggesting that there is no significant overdispersion in the GPR models. The adjusted percent deviance explained is 0.44 for R1 and 0.58 for R2, which means that the selected built-environment variables can explain 44% and 58% of the variance in R1 and R2.

Further, the regression coefficients indicate that private residential density has a positive association with both R1 and R2, which means that areas with higher private residential density tend to have a higher COVID-19 risk. Population density, however, has a negative association with both R1 and R2. Transport facility density and building height have positive associations with R1, while land-use diversity has a negative association with R1. Green space density has a positive association with R2, which means that higher green space density tends to increase the visiting frequency of the confirmed cases. The reason is that green space is likely to attract people to undertake various outdoor activities and these people include some of the confirmed cases. Moreover, sky view has a negative association with R2, which suggests that areas with better sky view have lower risk assessed with R2. The result means that a higher possibility of seeing the sky tends to reduce the risk of COVID-19.

Table 3. Global Poisson regression (GPR) results.

GPR Model (R1)					
Variable	Abbreviations	Coef.	S.E.	*p*-value	VIF
Transport facilities density	TF	2.50	0.54	0.000 ***	3.84
Population density	PD	−4.00	0.48	0.000 ***	2.35
Private residential	PR	3.21	0.74	0.000 ***	2.76
Land-use diversity	LUD	−1.13	0.19	0.000 ***	1.78
Building height	BH	0.90	0.37	0.015 **	4.68
Residual deviance = 97					
Degrees of freedom = 96					
AIC = 331.21					
Adjusted percent deviance explained = 0.44					
GPR Model (R2)					
Variable	Abbreviations	Coef.	S.E.	*p*-value	VIF
Nodal accessibility	NA	1.78	0.11	0.000 ***	2.48
Population density	PD	−1.59	0.17	0.000 ***	3.32
Private residential	PR	2.58	0.28	0.000 ***	2.82
Commercial density	CD	1.98	0.40	0.000 ***	1.27
Green space density	GSD	0.95	0.15	0.000 ***	2.03
Sky view	SV	−4.82	0.42	0.000 ***	4.17
Residual deviance = 187					
Degrees of freedom = 181					
AIC = 1513.14					
Adjusted percent deviance explained = 0.58					

* Represents statistically significant at the $p < 0.1$ level. ** Represents statistically significant at the $p < 0.05$ level. *** Represents statistically significant at the $p < 0.01$ level.

4.3. The Relationship between Built-Environment Features and COVID-19 Risk: Results of the GWPR Analysis

In this subsection, we examine the relationship between the built-environment variables and COVID-19 risk based on the results of the GWPR models. The values of the bandwidth estimated by the models are 66 and 55 for R1 and R2, respectively. Table 4 shows the results of the relative performance of the GPR and GWPR models. As the table indicates, the adjusted percent deviance explained by the GWPR models (0.63 for R1 and 0.74 for R2) are higher than those of the GPR models (i.e., 0.44 for R1 and 0.58 for R2). Moreover, the Akaike information criterion (AIC) of the GWPR models (i.e., 149.42 for R1 and 512.93 for R2) are remarkably lower than those of the GPR models (429.71 for R1 and 1513.14 for R2). The improvement in adjusted percent deviance explained and the reduction in the AIC values indicate that the GWPR models have better explanatory power than the GPR models for examining the influence of the built-environment features on COVID-19 risk in Hong Kong.

Table 4. Comparison of the global Poisson regression (GPR) and geographically weighted Poisson regression (GWPR) models.

	Goodness of Fit		
Model	**AIC**	**Percent Deviance Explained**	**Adjusted Percent Deviance Explained**
R1			
GPR	429.71	0.46	0.44
GWPR	149.42	0.71	0.63
R2			
GPR	1513.14	0.59	0.58
GWPR	512.93	0.81	0.74

Figure 6 presents the spatial distributions of local percent deviance explained by the GPWR models for R1 and R2. The results show that the two GPWR models present similar spatial distributions of local percent deviance explained in the north and western parts of the study area. Meanwhile, it can be observed that the GPWR models have lower explanatory power for R1 and R2 in the TPUs of and around Kwun Tong (marked as A in Figure 6a) and Mong Kok (marked as A in Figure 6b), respectively.

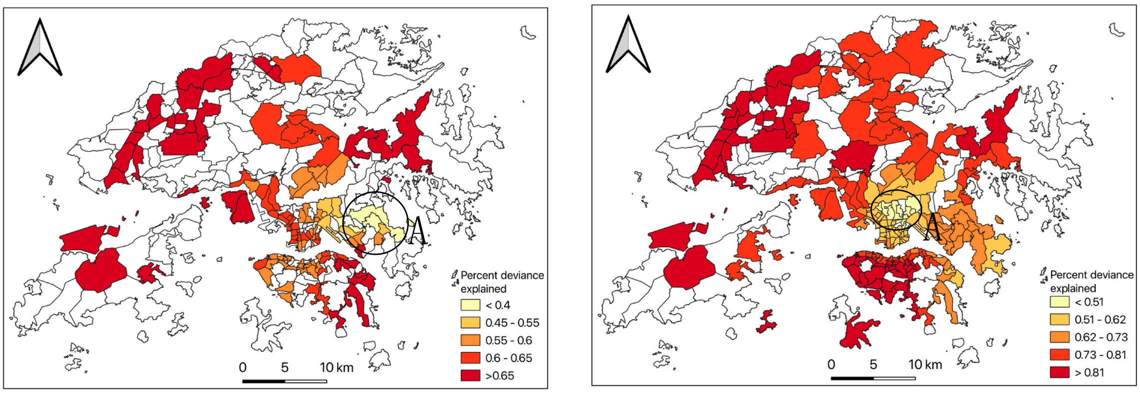

(**a**) (**b**)

Figure 6. Spatial distribution of local percent deviance explained by the GPWR models for R1 and R2: (**a**) Local percent deviance explained R1; (**b**) Local percent deviance explained R2.

Figure 7 shows the spatial distributions of the standard residuals from the two GPWR models for R1 and R2; 95% and 96% of the standard residuals have values in the range of (−2.58, 2.58), respectively. We further examine the spatial autocorrelation of the standard residuals and obtain the global Moran's *I* for the standard residuals of the GPWR models, which are −0.03 and −0.02, respectively, revealing that the distributions of the standard residuals from the GPWR models are random at the 5% level of significance. Moreover, the low values of the global Moran's *I* also indicate that there is no systematic error in the models.

The spatial distribution of the estimated coefficients of the built-environment variables is presented in Figures 8 and 9. The blue color signifies that the corresponding built-environment variable has a negative influence on COVID-19 risk, while the red color indicates a positive influence. The GWPR models reveal the spatially varying influence of each built-environment variable on COVID-19 risk. In Figure 8, it can be observed that the associations between transport facility density, population density, private residential density, land-use diversity, and building height, and COVID-19 risk fluctuate from negative to positive for R1. For variables such as transport facility density, private residential density, and building height, the proportions of TPUs with positive and negative coefficients are comparable to each other, which implies a complicated relationship between these variables and R1. For instance, the positive values for transport facility density, private residential density, and building height are mainly distributed in the downtown area and Tung Chung, while the negative values are found largely in the peripheral suburban areas (Figure 8a,c,e). Regarding population density, most TPUs in Hong Kong exhibit negative associations with R1, while the TPUs with positive associations only cover the village clusters in Ma On Shan (Figure 8b). Similarly, land-use diversity has a negative relationship with R1 for most TPUs (Figure 8d).

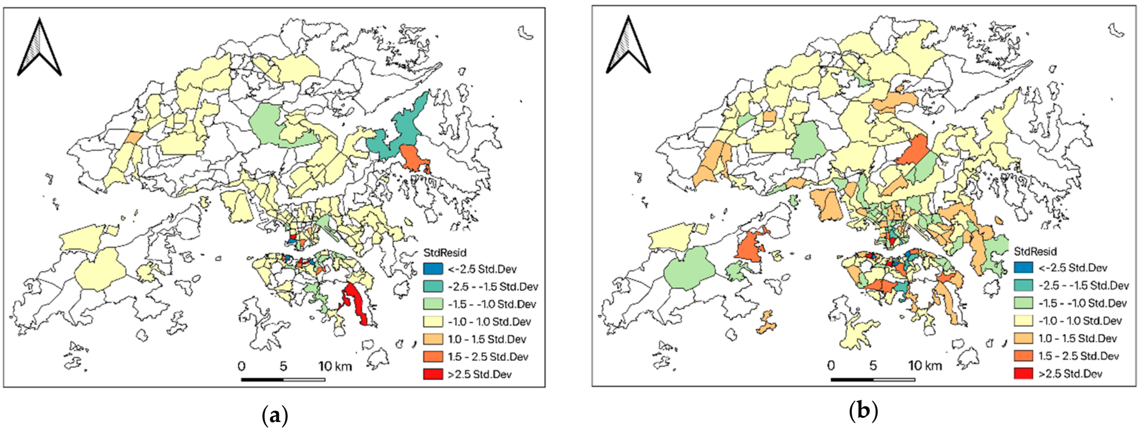

Figure 7. Spatial distribution of local standard residual from the GPWR models for R1 and R2: (**a**) Local standard residual R1; (**b**) Local standard residual R2.

Figure 9a indicates that nodal accessibility has a positive association with R2 for the entire study area, and higher associations are located in Hong Kong Island, Lamma Island, and Tin Shui Wai. Private residential density has a positive association with R2 for most TPUs (Figure 9c). Further, the associations between population density (Figure 9b), commercial density (see Figure 9d), green space density (Figure 9e) and sky view (Figure 9f) and R2 fluctuate from negative to positive. The proportions of TPUs with positive and negative coefficients are comparable to each other, which indicates a complex relationship between these variables and R2. For example, the positive values for green space (which includes hills, mountains, and country parks for hiking or picnicking) are mainly distributed in suburban areas, while the negative values are found in areas such as Central, Tsim Sha Tsui, and Wan Chai, where the density of pubs, restaurants, and shopping malls is high. Sky view and population density have similar patterns of values distribution: positive in the western part of Hong Kong and negative in the eastern part of Hong Kong.

In summary, the associations between the selected built-environment features and COVID-19 risk vary spatially across the study area. The GPR models provide the global relationship between the built-environment features and COVID-19 risk for the TPUs, and the GWPR models reveal some distinctive and complex differences among the TPUs by considering spatial autocorrelation and spatial nonstationarity. The model results shed light on the relationships between built-environment variables and COVID-19 risk at a more microscopic scale.

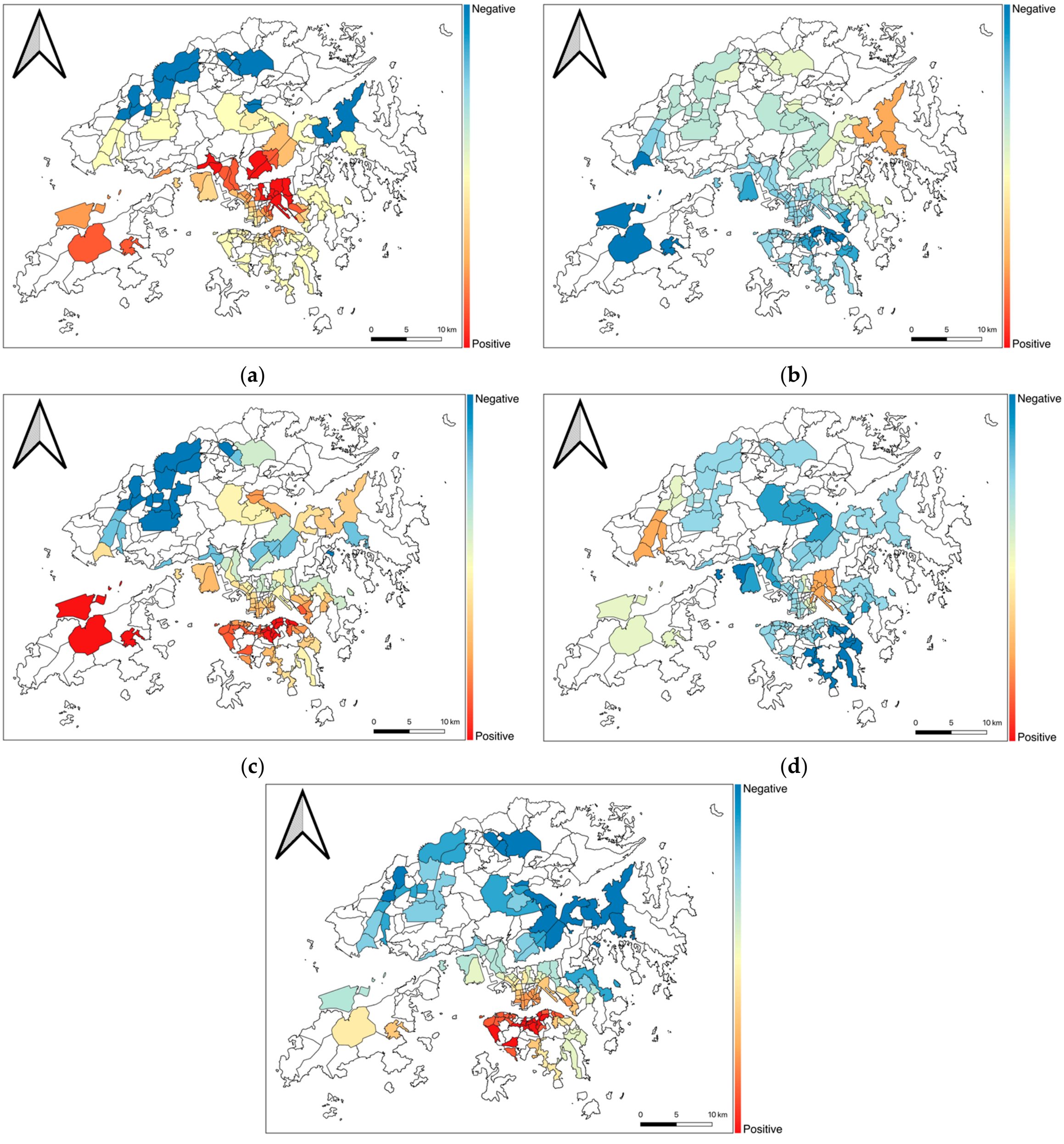

Figure 8. Spatial distribution of GWPR coefficients for R1: (**a**) Transport facility density; (**b**) Population density; (**c**) Private residential density; (**d**) Land-use diversity; (**e**) Building height.

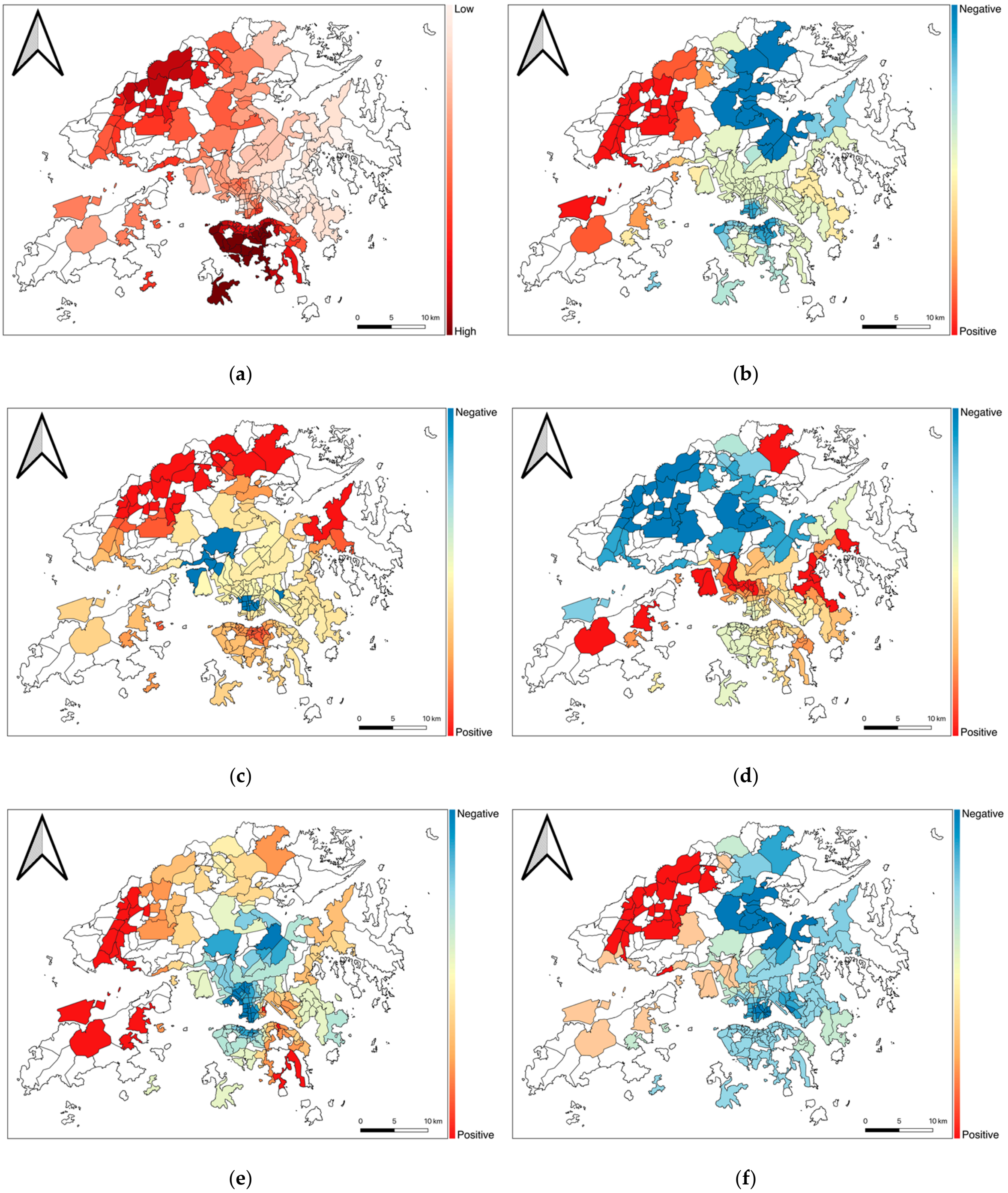

Figure 9. Spatial distribution of GWPR coefficients for R2: (**a**) Nodal accessibility; (**b**) Population density; (**c**) Private residential density; (**d**) Commercial density; (**e**) Green space density; (**f**) Sky view.

5. Discussion and Conclusions

Understanding the relationship between the built environment and COVID-19 risk could support health authorities to respond to the pandemic. In this paper, we utilized GPR and GWPR models to investigate the relationship between built-environment features and COVID-19 risk in Hong Kong at the TPU level. The risk of COVID-19 is assessed using the incidence rate (R1) and venue density (R2). The main findings of the study are summarized as follows.

First, both R1 and R2 have a remarkable decay effect over space. It implies that there are a few areas with a high COVID-19 risk. Similar results have been observed in the studies by Desjardins et al. [53]

and Gatto et al. [54] in the U.S. and Italy in the early stage of the pandemic. Further, the rate of decay of R1 is higher than that of R2, reflecting that the number of TPUs with a high R1 is smaller than the number of TPUs with a high R2. This implies that the incidence rate indicator may underestimate the COVID-19 risk in some suburban areas with a large area of public space. Second, the GPR model results reveal a close relationship between selected built-environmental variables and COVID-19 risk. Note that Nguyen et al. [55] reported similar results by using large Google Street View image datasets on American neighborhoods (i.e., zip code area). They found that land-use diversity and higher accessibility have positive associations with higher COVID-19 cases without considering spatial nonstationarity. Meanwhile, our results show a negative association between population density and the risk of COVID-19. The result differs from those of the studies of Amram et al. [56] and Xiong et al. [57] in the U.S. and China (i.e., population density has a positive or nonsignificant association with COVID-19 risk). These conflicting results raise several hypotheses that are worth discussing. First of all, as we mentioned in Section 2, using different spatial scales of the analytical units or geographic areas (e.g., counties, census tracts, or census block groups) in the analysis may lead to different results (i.e., the modifiable areal unit problem). Then, several other variables could potentially prevent disease transmission over the neighborhoods in a dense and developed city. For instance, dense areas in a developed city may have better access to health care facilities and better adherence to social distancing by residents (e.g., more than 97.5% of the people in Hong Kong wore a mask when they went out and more than 85% of them avoided crowded places during February and March 2020 [58]).

Taking into account spatial nonstationarity, our results present that the GWPR models perform better than GPR models based on the value of adjusted percent deviance explained and AIC. The low global Moran's I values (R1: −0.03; R2: −0.02) in the residual maps indicate that there is no systematic error in the models. The results show that the relationships between selected built-environmental variables and COVID-19 risk (i.e., R1 and R2) vary spatially across the study area. For built-environment features such as transport facility density, private residential density, building height, population density, commercial density, green space density, and sky view, the relative proportions of TPUs with positive and negative coefficients indicate a complicated relationship between selected built-environment variables and COVID-19 risk.

Based on the results of the two sets of regression models, we observed the complex relationships between selected built-environment variables and COVID-19 risk. The results also suggest other interesting observations that are worth discussing. For instance, most of the confirmed cases who lived in Tung Chung were actually infected in their workplaces (i.e., Central). It implies that the strong spatial interactions between suburban areas (e.g., Tung Chung) and the downtown area (e.g., Central) may result in similar patterns in COVID-19 risk (e.g., transport facility density for R1 and nodal accessibility for R2). Moreover, green space density and sky view in the downtown area (e.g., Central and Tsim Sha Tsui) and some suburban areas (e.g., Tung Chung and Tuen Mun) have opposite effects on COVID-19 risk.

Our findings have several important implications for non-pharmaceutical intervention measures for the government during the pandemic. First, the results of the frequency and spatial distributions of COVID-19 risk indicate that a few TPUs have a higher COVID-19 risk. Health authorities should thus focus on these areas for follow-up interventions in order to control the COVID-19 pandemic. Second, the results suggest that the incidence rate may underestimate the risk of COVID-19 in some suburban areas with large areas of public recreational space (e.g., parks). On one hand, areas with dense transport facilities, higher nodal accessibility, more green space, and a good sky view tend to attract more visitors. On the other hand, people who live in suburban areas may have to go to work in the downtown area, which has a higher risk. Moreover, the GPR and GWPR models indicate that dynamic interventions of COVID-19 transmission risk should be considered during the pandemic. For instance, restricting people from going to the country parks and certain residential areas in the suburb or limiting group activities in these areas may help control the pandemic.

In this study, we found that the spatial patterns of built-environment features influence the spatial patterns of COVID-19 risk across the study area. The findings suggest that COVID-19 can be explained by pertinent built-environment features. The methods used in the study can be applied to other cities in the world to investigate the relationship between the built environment and COVID-19 risk. Comparative studies would be helpful in revealing the effects of different human behaviors and intervention measures in different sociocultural contexts. This is a fruitful possible direction for future research.

Meanwhile, there are several limitations in this study. First, the study used COVID-19 data from 27 January to 14 April 2020, during which the Hong Kong Government had implemented several non-pharmaceutical intervention measures in response to the COVID-19 pandemic. The results from our regression models thus captured the relationship between built-environment features and COVID-19 risk under these non-pharmaceutical interventions. It is unclear whether the relationship between the built environment and COVID-19 risk we identified will also hold under normal times (i.e., without intervention measures). In the future, we plan to explore this in the post-pandemic period. Second, this study used the incidence rate and venue density as measures of COVID-19 risk. Other indicators, such as the decrease in survived coronavirus estimated based on the last visiting time by confirmed cases, could be considered in the future. As the decay effect of coronavirus survival over time is related to different environmental surfaces, incorporating this variable into the analysis may provide more insights into COVID-19 risk and its relationship with specific types of built environments. Third, this study did not consider the temporal dynamics of the spatial interaction among TPUs (e.g., the spatial interactions among TPUs may change between different times of a day or before and after the implementation of intervention policies), which may lead to different associations between the built environment and COVID-19 risk.

Author Contributions: Jianwei Huang, Mei-Po Kwan, and Zihan Kan conceived and designed the study. Jianwei Huang collected the data and conducted data analysis. Man Sing Wong, Coco Yin Tung Kwok, and Xinyu Yu processed the data. Jianwei Huang, Mei-Po Kwan, and Zihan Kan interpreted the results. Jianwei Huang and Mei-Po Kwan wrote the original draft. Jianwei Huang, Mei-Po Kwan, Zihan Kan, Man Sing Wong, Coco Yin Tung Kwok, and Xinyu Yu revised the manuscript. All authors have read and agreed to the published version of the manuscript.

Funding: This research was supported by a grant from the Research Committee on Research Sustainability of Major RGC Funding Schemes of the Chinese University of Hong Kong (Grant no. 3133240). Dr. Man Sing Wong thanks the funding support from a grant by the General Research Fund (Grant no. 15602619), and the Research Institute for Sustainable Urban Development (Grant no. 1-BBWD), the Hong Kong Polytechnic University.

Conflicts of Interest: The authors declare no conflict of interest.

References

1. Guarner, J. Three emerging coronaviruses in two decades: The story of SARS, MERS, and now COVID-19. *Am. J. Clin. Pathol.* **2020**, *153*, 420–421. [CrossRef]
2. World Health Organization. Novel Coronavirus (COVID-19) Situation Report-75. 2020. Available online: https://www.who.int/docs/default-source/coronaviruse/situation-reports/20200404-sitrep-75-covid-19.pdf?sfvrsn=99251b2b_2 (accessed on 12 May 2020).
3. Kupferschmidt, K.; Cohen, J. China's Aggressive Measures Have Slowed the Coronavirus. They May not Work in Other Countries. 2020. Available online: https://www.sciencemag.org/news/2020/03/china-s-aggressive-measures-have-slowed-coronavirus-they-may-not-work-other-countries (accessed on 12 May 2020).
4. Tian, H.; Liu, Y.; Li, Y.; Wu, C.H.; Chen, B.; Kraemer, M.U.; Li, B.; Cai, J.; Xu, B.; Yang, Q.; et al. An investigation of transmission control measures during the first 50 days of the COVID-19 epidemic in China. *Science* **2020**, *368*, 638–642. [CrossRef] [PubMed]
5. Koo, J.R.; Cook, A.R.; Park, M. Interventions to mitigate early spread of COVID-19 in Singapore: A modelling study. *Lancet Infect Dis.* **2020**, *20*, 678–688. [CrossRef]
6. Wilder-Smith, A.; Freedman, D.O. Isolation, quarantine, social distancing and community containment: Pivotal role for old-style public health measures in the novel coronavirus (2019-nCoV) outbreak. *J. Travel Med.* **2020**, *27*, taaa020. [CrossRef]

7. Del Valle, S.; Hethcote, H.; Hyman, J.M.; Castillo-Chavez, C. Effects of behavioral changes in a smallpox attack model. *Math. Biosci.* **2005**, *195*, 228–251. [CrossRef]
8. Fenichel, E.P.; Castillo-Chavez, C.; Ceddia, M.G.; Chowell, G.; Parra, P.A.G.; Hickling, G.J.; Holloway, G.; Horan, R.; Morin, B.; Perrings, C.; et al. Adaptive human behavior in epidemiological models. *Proc. Natl. Acad. Sci. USA* **2011**, *108*, 6306–6311. [CrossRef] [PubMed]
9. Yang, Y.; Atkinson, P.M.; Ettema, D. Analysis of CDC social control measures using an agent-based simulation of an influenza epidemic in a city. *BMC Infect. Dis.* **2011**, *11*, 199. [CrossRef] [PubMed]
10. Rizzo, A.; Frasca, M.; Porfiri, M. Effect of individual behavior on epidemic spreading in activity-driven networks. *Phys. Rev. E* **2014**, *90*, 042801. [CrossRef] [PubMed]
11. World Health Organization. Non-Pharmaceutical Public Health Measures for Mitigating the Risk and Impact of Epidemic and Pandemic Influenza: Annex: Report of Systematic Literature Reviews. 2019. Available online: https://apps.who.int/iris/bitstream/handle/10665/329439/WHO-WHE-IHM-GIP-2019.1-eng.pdf (accessed on 12 May 2020).
12. Bayham, J.; Fenichel, E.P. Impact of school closures for COVID-19 on the US health-care workforce and net mortality: A modelling study. *Lancet Public Health* **2020**, *5*, e271–e278. [CrossRef]
13. Douglas, M.; Katikireddi, S.V.; Taulbut, M.; McKee, M.; McCartney, G. Mitigating the wider health effects of covid-19 pandemic response. *BMJ Br. Med. J.* **2020**, *369*, m1557. [CrossRef]
14. Venkatesh, A.; Edirappuli, S. Social distancing in covid-19: What are the mental health implications? *BMJ Br. Med. J.* **2020**, *369*, m1379. [CrossRef] [PubMed]
15. Galea, S.; Merchant, R.M.; Lurie, N. The mental health consequences of COVID-19 and physical distancing: The need for prevention and early intervention. *JAMA Intern. Med.* **2020**, *180*, 817–818. [CrossRef] [PubMed]
16. Emeruwa, U.N.; Ona, S.; Shaman, J.L.; Turitz, A.; Wright, J.D.; Gyamfi-Bannerman, C.; Melamed, A. Associations between Built Environment, Neighborhood Socioeconomic Status, and SARS-CoV-2 Infection among Pregnant Women in New York City. *JAMA Netw.* **2020**, *324*, 390–392. [CrossRef] [PubMed]
17. Frank, L.D.; Engelke, P.O. The built environment and human activity patterns: Exploring the impacts of urban form on public health. *J. Plan. Lit.* **2001**, *16*, 202–218. [CrossRef]
18. Hamidi, S.; Sabouri, S.; Ewing, R. Does Density Aggravate the COVID-19 Pandemic? Early Findings and Lessons for Planners. *J. Am. Plann. Assoc.* **2020**, 1–15. [CrossRef]
19. Weber, D.J.; Rutala, W.A.; Fischer, W.A.; Kanamori, H.; Sickbert-Bennett, E.E. Emerging infectious diseases: Focus on infection control issues for novel coronaviruses (Severe Acute Respiratory Syndrome-CoV and Middle East Respiratory Syndrome-CoV), hemorrhagic fever viruses (Lassa and Ebola), and highly pathogenic avian influenza viruses, A (H5N1) and A (H7N9). *Am. J. Infect. Control* **2016**, *44*, e91–e100. [CrossRef]
20. Casanova, L.; Rutala, W.A.; Weber, D.J.; Sobsey, M.D. Survival of surrogate coronaviruses in water. *Water Res.* **2009**, *43*, 1893–1898. [CrossRef]
21. Peiris, J.S.M.; Chu, C.M.; Cheng, V.C.C.; Chan, K.S.; Hung, I.F.N.; Poon, L.L.; Law, K.I.; Tang, B.S.F.; Hon, T.Y.W.; Chan, C.S.; et al. Clinical progression and viral load in a community outbreak of coronavirus-associated SARS pneumonia: A prospective study. *Lancet* **2003**, *361*, 1767–1772. [CrossRef]
22. Van Doremalen, N.; Bushmaker, T.; Morris, D.H.; Holbrook, M.G.; Gamble, A.; Williamson, B.N.; Tamin, A.; Harcourt, J.L.; Thornburg, N.J.; Gerber, S.I.; et al. Aerosol and surface stability of SARS-CoV-2 as compared with SARS-CoV-1. *N. Engl. J. Med.* **2020**, *382*, 1564–1567. [CrossRef]
23. Handy, S.L.; Boarnet, M.G.; Ewing, R.; Killingsworth, R.E. How the built environment affects physical activity: Views from urban planning. *Am. J. Prev. Med.* **2002**, *23*, 64–73. [CrossRef]
24. Yan, J.; Grantham, M.; Pantelic, J.; de Mesquita, P.J.B.; Albert, B.; Liu, F.; Ehrman, S.; Milton, D.K.; EMIT Consortium. Infectious virus in exhaled breath of symptomatic seasonal influenza cases from a college community. *Proc. Natl. Acad. Sci. USA* **2018**, *115*, 1081–1086. [CrossRef]
25. Zhao, P.; Kwan, M.-P.; Zhou, S. The uncertain geographic context problem in the analysis of the relationships between obesity and the built environment in Guangzhou. *Int. J. Environ. Res. Public Health* **2018**, *15*, 308. [CrossRef]
26. Wang, J.; Lee, K.; Kwan, M.-P. Environmental influences on leisure-time physical inactivity in the US: An exploration of spatial non-stationarity. *ISPRS Int. J. Geoinf.* **2018**, *7*, 143. [CrossRef]
27. Huang, J.; Liu, X.; Zhao, P.; Zhang, J.; Kwan, M.P. Interactions between bus, metro, and taxi use before and after the Chinese Spring Festival. *ISPRS Int. J. Geoinf.* **2019**, *8*, 445. [CrossRef]

28. Zhao, P.; Xu, Y.; Liu, X.; Kwan, M.-P. Space-time dynamics of cab drivers' stay behaviors and their relationships with built environment characteristics. *Cities* **2020**, *101*, 102689. [CrossRef]
29. Rundle, A.; Neckerman, K.M.; Freeman, L.; Lovasi, G.S.; Purciel, M.; Quinn, J.; Richards, C.; Sircar, N.; Weiss, C. Neighborhood food environment and walkability predict obesity in New York City. *Environ. Health Perspect.* **2009**, *117*, 442–447. [CrossRef] [PubMed]
30. Bodor, J.N.; Rice, J.C.; Farley, T.A.; Swalm, C.M.; Rose, D. The association between obesity and urban food environments. *J. Urban Health* **2010**, *87*, 771–781. [CrossRef] [PubMed]
31. Lu, Y. Using Google Street View to investigate the association between street greenery and physical activity. *Landsc. Urban Plan.* **2019**, *191*, 103435. [CrossRef]
32. Lin, T.P.; Tsai, K.T.; Hwang, R.L.; Matzarakis, A. Quantification of the effect of thermal indices and sky view factor on park attendance. *Landsc. Urban Plan.* **2012**, *107*, 137–146. [CrossRef]
33. Carter, S.J.; Baranauskas, M.N.; Fly, A.D. Considerations for obesity, vitamin D, and physical activity amidst the COVID-19 pandemic. *Obesity* **2020**, *28*, 1176–1177. [CrossRef] [PubMed]
34. Gallè, F.; Sabella, E.A.; Molin, G.D.; Giglio, O.D.; Caggiano, G.; Onofrio, V.D.; Ferracuti, S.; Montagna, M.T.; Liguori, G.; Orsi, G.B.; et al. Understanding Knowledge and Behaviors Related to CoViD-19 Epidemic in Italian Undergraduate Students: The EPICO Study. *Int. J. Environ. Res. Public Health* **2020**, *17*, 3481. [CrossRef] [PubMed]
35. Leyden, K.M. Social capital and the built environment: The importance of walkable neighborhoods. *Am. J. Public Health* **2003**, *93*, 1546–1551. [CrossRef] [PubMed]
36. Mouratidis, K. Built environment and social well-being: How does urban form affect social life and personal relationships? *Cities* **2018**, *74*, 7–20. [CrossRef]
37. Chen, H.; Jia, B.; Lau, S. Sustainable urban form for Chinese compact cities: Challenges of a rapid urbanized economy. *Habitat Int.* **2008**, *32*, 28–40. [CrossRef]
38. Pinter-Wollman, N.; Jelić, A.; Wells, N.M. The impact of the built environment on health behaviours and disease transmission in social systems. *Philos. Trans. R. Soc. Lond. B Biol. Sci.* **2018**, *373*, 20170245. [CrossRef]
39. Bajardi, P.; Poletto, C.; Ramasco, J.J.; Tizzoni, M.; Colizza, V.; Vespignani, A. Human mobility networks, travel restrictions, and the global spread of 2009 H1N1 pandemic. *PLoS ONE* **2011**, *6*, e16591. [CrossRef]
40. Chinazzi, M.; Davis, J.T.; Ajelli, M.; Gioannini, C.; Litvinova, M.; Merler, S.; Piontti, A.P.y.; Mu, K.; Rossi, L.; Sun, K.; et al. The effect of travel restrictions on the spread of the 2019 novel coronavirus (COVID-19) outbreak. *Science* **2020**, *368*, 395–400. [CrossRef]
41. Samuelsson, K.; Barthel, S.; Colding, J.; Macassa, G.; Giusti, M. Urban nature as a source of resilience during social distancing amidst the coronavirus pandemic. *OSF Prepr.* **2020**. [CrossRef]
42. Van Bavel, J.J.; Baicker, K.; Boggio, P.S.; Capraro, V.; Cichocka, A.; Cikara, M.; Crockett, M.J.; Crum, A.J.; Douglas, K.M.; Druckman, J.N.; et al. Using social and behavioural science to support COVID-19 pandemic response. *Nat. Hum. Behav.* **2020**, *4*, 460–471. [CrossRef] [PubMed]
43. Dietz, L.; Horve, P.F.; Coil, D.A.; Fretz, M.; Eisen, J.A.; Van Den Wymelenberg, K. 2019 novel coronavirus (COVID-19) pandemic: Built environment considerations to reduce transmission. *mSystems* **2020**, *5*, e00245-20. [CrossRef]
44. Feng, Y.; Marchal, T.; Sperry, T.; Yi, H. Influence of wind and relative humidity on the social distancing effectiveness to prevent COVID-19 airborne transmission: A numerical study. *J. Aerosol Sci.* **2020**, *147*, 105585. [CrossRef] [PubMed]
45. Yang, J.; Wong, M.S.; Menenti, M.; Nichol, J. Modeling the effective emissivity of the urban canopy using sky view factor. *ISPRS J. Photogramm. Remote Sens.* **2015**, *105*, 211–219. [CrossRef]
46. Oke, T.R. Street design and urban canopy layer climate. *Energy Build.* **1988**, *11*, 103–113. [CrossRef]
47. Lai, P.-C.; Low, C.-T.; Tse, W.-S.C.; Tsui, C.-K.; Lee, H.; Hui, P.-K. Risk of tuberculosis in high-rise and high density dwellings: An exploratory spatial analysis. *Environ. Pollut.* **2013**, *183*, 40–45. [CrossRef]
48. Alexander, C.; Ishikawa, S.; Silverstein, M. *A Pattern Language: Towns, Buildings, Construction*; Oxford University Press: Oxford, UK, 1977.
49. Lee, K.; Park, J.S.; Goh, S.; Choi, M. Accessibility measurement in transportation networks and application to the Seoul bus system. *Geogr. Anal.* **2019**, *51*, 339–353. [CrossRef]
50. Lee, K.; Lee, H.Y. A new algorithm for graph-theoretic nodal accessibility measurement. *Geogr. Anal.* **1998**, *30*, 1–14. [CrossRef]

51. Kauhl, B.; Heil, J.; Hoebe, C.J.; Schweikart, J.; Krafft, T.; Dukers-Muijrers, N.H. The spatial distribution of hepatitis C virus infections and associated determinants—An application of a geographically weighted Poisson regression for evidence-based screening interventions in hotspots. *PLoS ONE* **2015**, *10*, e0135656. [CrossRef]
52. Brunsdon, C.; Fotheringham, A.S.; Charlton, M.E. Geographically weighted regression: A method for exploring spatial nonstationarity. *Geogr Anal.* **1996**, *28*, 281–298. [CrossRef]
53. Desjardins, M.R.; Hohl, A.; Delmelle, E.M. Rapid surveillance of COVID-19 in the United States using a prospective space-time scan statistic: Detecting and evaluating emerging clusters. *Appl. Geogr.* **2020**, *118*, 102202. [CrossRef]
54. Gatto, M.; Bertuzzo, E.; Mari, L.; Miccoli, S.; Carraro, L.; Casagrandi, R.; Rinaldo, A. Spread and dynamics of the COVID-19 epidemic in Italy: Effects of emergency containment measures. *Proc. Natl. Acad. Sci. USA* **2020**, *117*, 10484–10491. [CrossRef]
55. Nguyen, Q.C.; Huang, Y.; Kumar, A.; Duan, H.; Keralis, J.M.; Dwivedi, P.; Meng, H.-W.; Brunisholz, K.D.; Jay, J.; Javanmardi, M.; et al. Using 164 Million Google Street View Images to Derive Built Environment Predictors of COVID-19 Cases. *Int. J. Environ. Res. Public Health* **2020**, *17*, 6359. [CrossRef]
56. Amram, O.; Amiri, S.; Lutz, R.B.; Rajan, B.; Monsivais, P. Development of a vulnerability index for diagnosis with the novel coronavirus, COVID-19, in Washington State, USA. *Health Place* **2020**, *64*, 102377. [CrossRef] [PubMed]
57. Xiong, Y.; Wang, Y.; Chen, F.; Zhu, M. Spatial Statistics and Influencing Factors of the COVID-19 Epidemic at Both Prefecture and County Levels in Hubei Province, China. *Int. J. Environ. Res. Public Health* **2020**, *17*, 3903. [CrossRef]
58. Cowling, B.J.; Ali, S.T.; Ng, T.W.; Tsang, T.K.; Li, J.C.; Fong, M.W.; Liao, Q.; Kwan, M.Y.; Lee, S.L.; Chiu, S.S.; et al. Impact assessment of non-pharmaceutical interventions against coronavirus disease 2019 and influenza in Hong Kong: An observational study. *Lancet Public Health* **2020**, *5*, e279–e288. [CrossRef]

Publisher's Note: MDPI stays neutral with regard to jurisdictional claims in published maps and institutional affiliations.